Selective oxidation of propylene to acrolein over supported V_2O_5/Nb_2O_5 catalysts: An *in situ* Raman, IR, TPSR and kinetic study

Chunli Zhao, Israel E. Wachs *

*Operando Molecular Spectroscopy & Catalysis Lab, Departments of Chemical Engineering and Chemistry,
Lehigh University, Bethlehem, PA 18015, United States*

Available online 24 August 2006

Abstract

The vapor-phase selective oxidation of propylene ($H_2C=CHCH_3$) to acrolein ($H_2C=CHCHO$) was investigated over supported V_2O_5/Nb_2O_5 catalysts. The catalysts were synthesized by incipient wetness impregnation of V-isopropoxide/isopropanol solutions and calcination at 450 °C. The catalytic active vanadia component was shown by *in situ* Raman spectroscopy to be 100% dispersed as surface VO_x species on the Nb_2O_5 support in the sub-monolayer region (<8.4 V/nm^2). Surface allyl species ($H_2C=CHCH_{2*}$) were observed with *in situ* FT-IR to be the most abundant reaction intermediates. The acrolein formation kinetics and selectivity were strongly dependent on the surface VO_x coverage. Two surface VO_x sites were found to participate in the selective oxidation of propylene to acrolein. The reaction kinetics followed a Langmuir–Hinshelwood mechanism with first-order in propylene and half-order in O_2 partial pressures. C_3H_6-TPSR spectroscopy studies also revealed that the lattice oxygen from the catalyst was not capable of selectively oxidizing propylene to acrolein and that the presence of gas phase molecular O_2 was critical for maintaining the surface VO_x species in the fully oxidized state. The catalytic active site for this selective oxidation reaction involves the bridging V–O–Nb support bond.
© 2006 Elsevier B.V. All rights reserved.

Keywords: Spectroscopy; *In situ*; Raman; IR; TPSR; Catalyst; Metal oxide; Supported; Vanadium oxide; V_2O_5; Niobium oxide; Nb_2O_5; Oxidation; Selective; Propylene; Acrolein; Kinetics; TOF

1. Introduction

Acrolein ($CH_2=CHCHO$) ranks among the top industrial chemical intermediates produced annually and is currently manufactured via catalytic partial oxidation of propylene ($CH_2=CHCH_3$) [1,2]. The catalytic selective oxidation of propylene to acrolein has been extensively investigated since the 1960s and a number of bulk metal oxide catalysts have been found to be selective for this reaction: Bi–Mo–O [3–7], Mo–Te–O [8], Sn–Sb–O [9], U–Sb–O [10], Fe–Sb–Ti–O [11], Co–Fe–Mo–O [12] and cuprous oxide catalysts [13]. In contrast to the extensive literature studies reported for bulk mixed metal oxide catalysts (especially Bi–Mo–O), only one publication has examined propylene oxidation to acrolein over supported metal oxide catalysts. Desikan et al. investigated the catalytic properties of supported molybdenum oxide catalysts for

propylene oxidation and found that the characteristics of the surface molybdenum oxide catalytic active sites were overshadowed by the surface acidic properties of the oxide supports [14].

The current understanding of the mechanism and kinetics of the selective catalytic oxidation of propylene to acrolein is based on extensive investigations with bulk mixed metal oxides that primarily employed bulk Bi–Mo–O catalysts. This reaction has been shown to follow the Mars-van Krevelen reaction mechanism where the propylene methyl α-hydrogen is initially abstracted to form a symmetric allyl surface intermediate that subsequently reacts with bulk lattice oxygen from the catalyst to form the acrolein product [7,15–18]. The rate-determining-step involves bulk lattice oxygen diffusion at modest temperatures and methyl C–H bond breaking at high temperatures [19,20] Raman studies employing isotopic oxygen exchange studies confirmed that propylene oxidation over Bi–Mo–O catalyst involves the participation of bulk lattice oxygen [21]. Different reaction mechanism, however, have been proposed for propylene oxidation to acrolein over Bi–Mo–O [22,23] and there is a lack of

* Corresponding author. Tel.: +1 610 758 4274; fax: +1 610 758 5057.
  E-mail address: iew0@lehigh.edu (I.E. Wachs).

agreement among various investigators about the roles of the individual components of the catalyst with regard to the specific sites that activate propylene and insert oxygen.

There is presently intense interest in developing catalytic technologies for the selective catalytic oxidation of the more stable propane ($CH_3CH_2CH_3$) molecule to oxygenates such as acrolein (Acr: CH_2=CHCHO) and acrylic acid (AA: CH_2=CHCOOH). Vanadium-based catalysts, such as bulk mixed Mo–V–Te–Nb–O metal oxides, have been found to be able to activate propane for the selective formation of acrylic acid [24–26]. Many studies have concluded that the vanadia sites are the catalytic active sites responsible for selectively activating propane during its oxidation over these bulk mixed metal oxide catalysts [27–29]. The selective catalytic oxidation of propane to acrylic acid has been shown to proceed by the following series reaction network over bulk mixed Mo–V–Te–Nb–O metal oxides [30]:

$$CH_3CH_2CH_3 \rightarrow CH_2{=}CHCH_3 \rightarrow CH_2{=}CHCHO$$
$$\rightarrow CH_2{=}CHCOOH.$$
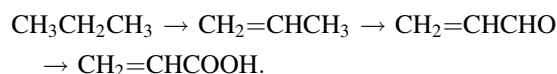
The selective oxidative dehydrogenation of propane to propylene, the first step of the propane oxidation reaction network, has already been investigated over model well-defined supported vanadium oxide catalysts where the molecular and electronic structures of the surface vanadia sites could be directly monitored with *in situ* spectroscopic techniques (Raman, IR and UV–vis) [31–36] These model studies revealed that this reaction proceeded via the Mars-van Krevelen mechanism and the catalytic active sites were the surface V^{5+} species possessing VO_4 coordination with one terminal V=O bond and three bridging V–O–V or V–O-support bonds [37–39]. The critical oxygen involved in the activation of propane rate determining step (rds) is in the bridging V–O-support bond [38,39].

The selective oxidation of propylene to acrolein, the second step of the propane oxidation reaction network over model well-defined supported vanadia catalysts, however, has not been investigated so far. The much higher activity of the surface vanadium oxide redox sites relative to surface molybdenum oxide redox sites may be able to overcome or minimize the strong influence the surface acidic properties of the oxide supports for this selective oxidation reaction that was previously encountered with supported molybdenum oxide catalysts [14]. The objective of the present study is to obtain fundamental insights into the nature of the catalytic active sites, surface reaction intermediates, and reaction mechanism and kinetics during the selective oxidation of propylene to acrolein over model well-defined supported vanadia catalysts where all the catalytic surface vanadia active sites are 100% dispersed on the support below monolayer surface coverage [34,35,37–39]. The supported V_2O_5/Nb_2O_5 catalyst system was chosen for this investigation because it consists of two of the significant components present in the bulk Mo–V–Te–Nb–O mixed metal oxide system being intensively investigated for propane oxidation.

2. Experimental

2.1. Catalyst preparation

The supported V_2O_5/Nb_2O_5 catalysts were prepared by the incipient wetness impregnation method. The vanadium tri-isopropoxide ($VO(OC_3H_7)_3$, Alfa, 95–98% purity) precursor and Nb_2O_5 (Niobium Products Co., S_{BET} 59 m^2/g) support were employed as the sources of vanadia and niobia. The synthesis was performed in a nitrogen environment and the precursor was dissolved in isopropanol (Fisher ACS, 99.9% pure) due to the moisture- and air-sensitive nature of the vanadium alkoxide precursor. The precursor-isopropanol solution, corresponding to the incipient wetness impregnation volume, was thoroughly mixed with the oxide support in a glove box under flowing N_2 and maintained in the glove box overnight at room temperature. The samples were subsequently dried at 120 °C for 1 h and 300 °C for 1h in flowing N_2, and were finally calcined in flowing air at 300 °C for 1 h and then for another 2 h at 450 °C to fully oxidize the supported vanadia component.

2.2. BET specific surface area

The specific surface areas of the samples were determined by nitrogen adsorption and desorption isotherms employing a Quantasorb surface area analyzer (Quantachrome Corporation, Model OS-9) using a 3:7 ratio of a N_2/He mixture. Typically, 0.1–0.3 g of sample was used for the measurement and the sample was outgassed at 200 °C prior to N_2 adsorption at -195.8 °C. The specific surface areas of the Nb_2O_5 support in the different vanadia loading samples were also determined by assuming that the added vanadium oxides do not contribute to the surface area of the samples since they are essentially dispersed as two-dimensional metal oxide overlayers on the Nb_2O_5 surface (confirmed with Raman spectroscopy) and only contribute to the mass of the sample.

2.3. Raman spectroscopy

The Raman spectra of the supported vanadia catalysts under dehydrated and *in situ* conditions were obtained with a UV/vis Raman spectrometer system (Horiba-Jobin Yvon LabRam-HR). The system possesses a confocal microscope (Olympus BX-30), a notch filter (532 nm) and single stage monochromator (LabRam-HR) with 900 grooves/mm grating. The scattered photons were directed and focused onto a single stage monochromater possessing a sensitive LN_2 CCD detector (JY-CCD3000). The spectra were collected in the 100–1800 cm^{-1} region with 532 nm excitation supplied by a Nd-YAG laser (10 mW). Typically, only 5–10 mg of the supported vanadia catalysts was placed into an *in situ* environmentally controlled cell (Linkam TS-1500) as loose powder, and the laser power was typically kept below 0.5 mW to minimize any laser induced sample changes and the spectrometer resolution was ~2 cm^{-1}. The dehydrated Raman spectra were obtained with 10 s/scan for 10 scans after heating the catalyst sample to 450 °C for 1 h in flowing 10% O_2/He

(Scott specialty gases: O_2, 99.996% purity; He, ultrahigh purity) and cooling the sample down to room temperature in flowing dry gas.

The *in situ* Raman spectra during propylene oxidation were obtained by the following procedure. The sample was placed inside the *in situ* cell and heated to 450 °C for 30 min under flowing 10% O_2/He. The dehydrated Raman spectrum was collected after cooling the sample to 300 °C in flowing O_2/He for 30 min. After the above treatment, 10% O_2/He and 2.96% C_3H_6/He (Scott specially gases, C_3H_6, 99.996% in ultrahigh pure He) gases as well as their mixtures with varying C_3H_6/O_2 ratios (6:1; 1:1, and 1:3) were introduced into the Raman cell and the spectra were collected during propylene oxidation at 300 °C after reaching steady-state (typically ~30 min). The used catalyst was reoxidized in the flowing O_2/He mixture from 300 to 450 °C after the reaction was terminated, and the Raman spectra of the oxidized catalyst was also recorded at 10 s/scan for 10 scan with ~2 cm^{-1} resolution.

2.4. In situ FT-IR spectroscopy

The *in situ* IR experiments were performed with a Bio-Rad FTS-40A FTIR spectrometer equipped with a DTGS detector. The IR spectrometer was operated in the transmission mode employing 1 s/scan and 200 scans with a resolution of ~2 cm^{-1}. The *in situ* IR spectra during propylene oxidation and reduction were obtained on catalyst samples that were pressed into self-supporting wafers that were placed in a specially designed *in situ* cell [38]. The dehydration pretreatment consisted of initially heating the sample to 300 °C in vacuum (~10^{-4} to 10^{-5} Torr) followed by cooling to 30 °C. After the above treatment, a 1:4 C_3H_6/O_2 ratio mixture, produced from 2.96% C_3H_6/He and 10% O_2/He, was introduced into the IR cell. The IR spectra were collected at different temperatures (30, 70, 100, 150, 200, 250, and 300 °C) in the reactive gas environment after reaching steady state. The influence of reducing (2.96% C_3H_6/He) and oxidizing (10% O_2/He) environments were also monitored at different temperatures.

2.5. C_3H_6-temperature programmed surface reaction (TPSR) spectroscopy

The C_3H_6-TPSR experiments were performed on an Altamira Instruments temperature programmed system (AMI-200) equipped with an online quadrupole mass spectrometer (Dycor Dymaxion, DME200MS). Typically, ~100 mg of the V_2O_5/Nb_2O_5 (8.4 V/nm^2) catalyst was loaded into a U shaped quartz tube and initially calcined at 450 °C (Air Products, Ultra Zero Grade Air, 30 ml/min) for 40 min to remove adsorbed moisture and any adsorbed impurities that may be present. The pretreated sample was (i) cooled down in flowing air to 110 °C; (ii) the gas stream was subsequently switched to an ultra high purity helium flow upon further cooling to 50 °C, and (iii) maintained for 1/2 h at 50 °C to remove any physically adsorbed oxygen or background gases.

Propylene chemisorption was performed by flowing a 2.96% C_3H_6/He gas mixture (30 ml/min) for 30 min at 50 °C and the sample was again purged at the same temperature with flowing helium for an additional 1/2 h to remove any residual physically adsorbed C_3H_6. The TPSR experiments were then performed with a heating rate of 10 °C/min in either flowing UHP He or 5% O_2/He, and the desorbing products were monitored with the online quadrupole MS. The *m/e* values used to detect the different desorption products were *m/e* = 41 for C_3H_6, *m/e* = 56 for CH_2=CHCHO (acrolein), *m/e* = 43 for CH_3COCH_3 (acetone), *m/e* = 29 for CH_3CHO (acetaldehyde), *m/e* = 55 for CH_2=CHCOOH (acrylic acid), *m/e* = 28 for CO and *m/e* = 44 for CO_2. Unlike single crystal studies in vacuum, it is not possible to determine the kinetic parameters from the FWHM of the TPSR curve since the desorbing products signals becomes broadened due to dispersion of the gases as they pass through the thin catalyst bed. Consequently, only the T_p temperature during C_3H_6-TPSR can be accurately determined by use of the Redhead equation [40].

2.6. Steady-state oxidation of C_3H_6

The steady-state propylene oxidation reactions over supported vanadia catalysts were conducted in a vertical down-flow isothermal fixed-bed reactor (Pyrex glass tubing, 1/4 o.d. and 1 ft long) at atmospheric pressure. The temperature of the reactor and the catalyst bed were measured by two thermocouples located outside and inside the reactor tube just above the catalyst bed. The temperature was controlled by a Diqi PID temperature controller (series 2600). The reactor effluent was analyzed by an online Hewlett–Packard Gas Chromatograph (Agilent series 6890) equipped with both TCD and FID detectors. A Carboxene-1000 packed column and a Supelco capillary column were employed in parallel for the TCD and FID analysis, respectively.

The propylene, O_2 and helium flow rates were adjusted through separate mass flow controllers (Brooks Model 5850E Series) to control the propylene-to-oxygen ratio and maintaining a total flow rate of 100 cm^3/min. The O_2 and C_3H_6 reaction orders were examined by varying the reactant flow rates between 5 and 55 cm^3/min, and He was the balance gas to produce a total flow rate of 100 cm^3/min. Standard gases (Scotty special gas, 99.99% pure), including propylene and various reaction products were used for both G.C. peak identification and calibration.

The powdered catalysts were fixed by glass wool fiber in the reactor and the amount of the catalyst was varied depending on its activity and surface area in order to minimize heat and mass transfer effects. Typically between 10 and 30 mg of catalyst was employed for propylene oxidation. The experimental runs were performed from 250 to 400 °C and the C_3H_6 conversion was maintained below 2% to ensure differential reaction conditions. The catalytic activity, as measured by conversion and turnover frequency (TOF: the number of propylene molecules converted to acrolein per V atom per second), and selectivity values for each run were obtained.

Table 1
Specific surface areas (S_s) of supported V_2O_5/Nb_2O_5 catalysts, Nb_2O_5 support and surface vanadia density on Nb_2O_5 support

Supported V_2O_5/Nb_2O_5 catalysts	S_s of catalysts S_{BET} (m²/g)	S_s of Nb_2O_5 support of catalysts S_{BET} (m²/g)	Surface density of vanadia on Nb_2O_5 support (V atoms/nm²)
Nb_2O_5	59.5	59.5	0
2% V_2O_5/Nb_2O_5	56.8	58.0	2.3
3% V_2O_5/Nb_2O_5	56.2	57.9	3.5
5% V_2O_5/Nb_2O_5	51.4	54.1	5.9
7% V_2O_5/Nb_2O_5	47.0	50.5	8.4
9% V_2O_5/Nb_2O_5	38.4	42.2	11.1

3. Results

3.1. BET surface area and surface vanadia density

The BET surface areas of the supported vanadia-niobia catalysts and their corresponding surface vanadia densities (V/nm²) are presented in Table 1. Compared with the Nb_2O_5 support, all of the supported V_2O_5/Nb_2O_5 samples possess lower surface areas primarily due to the added mass of vanadium oxide. To better understand the effect of the added vanadium oxide on the Nb_2O_5 support surface area, the specific surface areas of the Nb_2O_5 support were also calculated by subtracting the vanadia contribution to the catalyst mass (see Table 1). The specific surface area of the Nb_2O_5 support monotonically decreases with increasing vanadia content due to sintering induced by the added vanadia during calcination. Based on the specific surface area of Nb_2O_5 support, the calculated corresponding surface vanadia density values for the supported V_2O_5/Nb_2O_5 catalysts were 2.3–11.1 V/nm².

3.2. Raman spectroscopy

3.2.1. Dehydrated Raman spectra

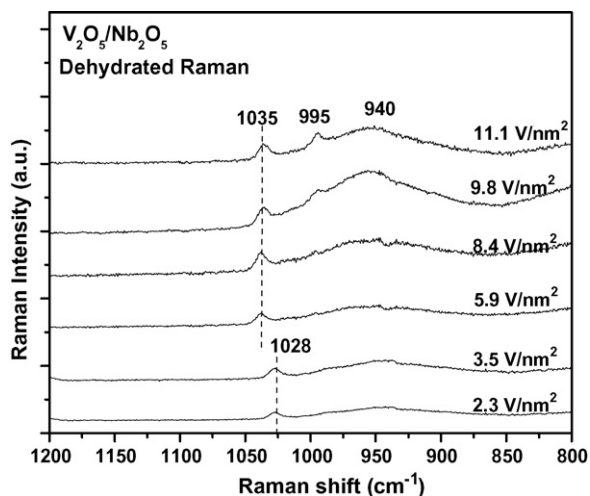Fig. 1 presents the Raman spectra for the dehydrated supported V_2O_5/Nb_2O_5 catalysts in the 800–1200 cm⁻¹ region.

The strong vibrations of bulk Nb_2O_5 were background subtracted in order to enhance the Raman bands of the supported vanadia phase. The appearance of crystalline V_2O_5 nanoparticles at ∼995 cm⁻¹ above 8 V/nm² reflects the completion of the surface VO_x monolayer phase, which is consistent with the prior literature conclusions for supported vanadia catalysts [37,39,41–43]. In the sub-monolayer region (<8.4 V/nm²), only vibrations from the surface VO_x species are present at 940 and 1028–1035 cm⁻¹. The 1028–1035 cm⁻¹ vibration originates from the terminal V=O bond and the 940 cm⁻¹ band arises from the bridging V–O–Nb bond [44–47]. The slight shift of the terminal V=O vibration from 1028 to 1035 cm⁻¹ with surface vanadia coverage has been associated with distortions of the dehydrated surface VO_x species with extent of polymerization of the surface VO_x species [48]. The Raman spectra of the dehydrated supported V_2O_5/Nb_2O_5 catalysts demonstrate that the supported vanadia phase is exclusively present as surface VO_x species, 100% dispersed, on the Nb_2O_5 support up to 8.4 V/nm², which corresponds to monolayer surface coverage.

3.2.2. In situ Raman spectroscopy during propylene oxidation

The in situ Raman spectra during propylene oxidation over the supported VO_x/Nb_2O_5 catalyst containing approximately monolayer surface vanadia coverage (8.4 V/nm²) are presented in Fig. 2 in the 800–1800 cm⁻¹ region. The strong vibrations of bulk Nb_2O_5 were background subtracted in order to enhance the Raman bands of the supported vanadia phase. The Raman intensity of the terminal V=O vibration at 1035 cm⁻¹ from the surface VO_x species decreases with the net reducing character of the reactive gas composition (increasing C_3H_6/O_2 ratio). This decrease in intensity is a consequence of the reduction of the surface V^{5+} species to V^{4+}/V^{3+} species, with the latter not being Raman active on the Nb_2O_5 support [39,48]. Surface carbonaceous deposits, Raman bands at ∼1400 and ∼1600 cm⁻¹, are also present during propylene oxidation when

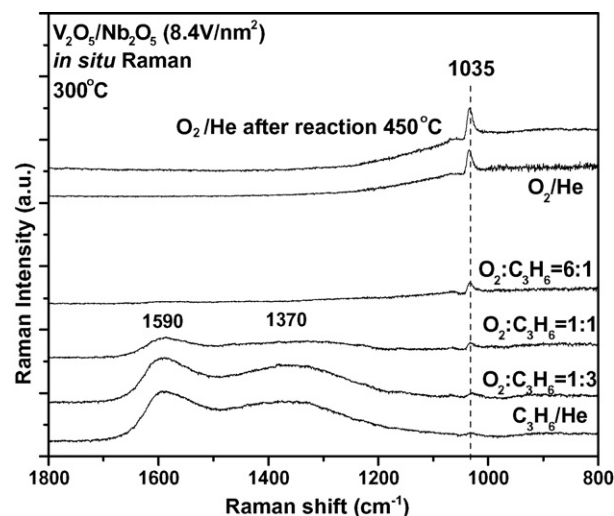Fig. 1. Raman spectra of dehydrated supported V_2O_5/Nb_2O_5 catalysts.

Fig. 2. In situ Raman spectra of supported V_2O_5/Nb_2O_5 (8.4 V/nm²) during propylene oxidation at 300 °C.

the O_2: C_3H_6 ratio becomes less than 1. The surface carbon residue is readily combusted in flowing O_2/He at 450 °C and the catalyst readily returns to its initial fully oxidized state.

3.3. In situ infrared spectroscopy

The *in situ* IR spectra during propylene oxidation over the monolayer supported V_2O_5/Nb_2O_5 (8.4 V/nm^2) catalyst during the C_3H_6 oxidation reaction in various temperatures condition are depicted in Fig. 3. The IR spectra of the oxidized samples before reaction are also shown for reference. Different regions of the IR spectra, 400–3600, 900–1350 and 2700–3600 cm^{-1} are depicted in Fig. 3a–c, respectively, for better clarity. For the oxidized catalyst in Fig. 3a, the sharp IR bands at 670/820 and 1035 cm^{-1} originate from the Nb–O support and surface V=O vibrations, respectively, and coincide with the corresponding Raman vibrations [45,49–51]. Weak and broad IR bands are also observed at ~1600 and 2048 cm^{-1} arising from physically adsorbed moisture and the V=O overtone vibration, respectively [52].

The IR vibration of the terminal V=O bond at ~1035 cm^{-1} broadens (see Fig. 3b), slightly decreases in intensity and shifts to lower wavenumber as the catalyst temperature is raised during propylene oxidation. These IR changes with reaction temperature are also reflected in the above Raman spectra and arise from structural changes of the surface VO_x species due to complexation with the surface reaction intermediates and reduction of the surface vanadia species. The weak IR band at ~913 cm^{-1}, present between 30 and 250 °C in Fig. 3b is characteristic of C–H wagging mode of C_3H_6 [53], and disappears above 250 °C because of the propylene desorption from the catalyst surface. New IR bands appear between 70 and 250 °C from C–H stretching (2987 cm^{-1}, see Fig. 3c), C–C stretching (1100 cm^{-1}, see Fig. 3b) and C=C (1673 cm^{-1}, see Fig. 3d) vibrations of surface reaction intermediates.

The IR difference spectra between the supported VO_x/Nb_2O_5 catalyst under reaction conditions and the fully oxidized dehydrated catalyst at 30 °C are shown in Fig. 3d in the 1050–1800 cm^{-1} region, in order to emphasize the vibrational
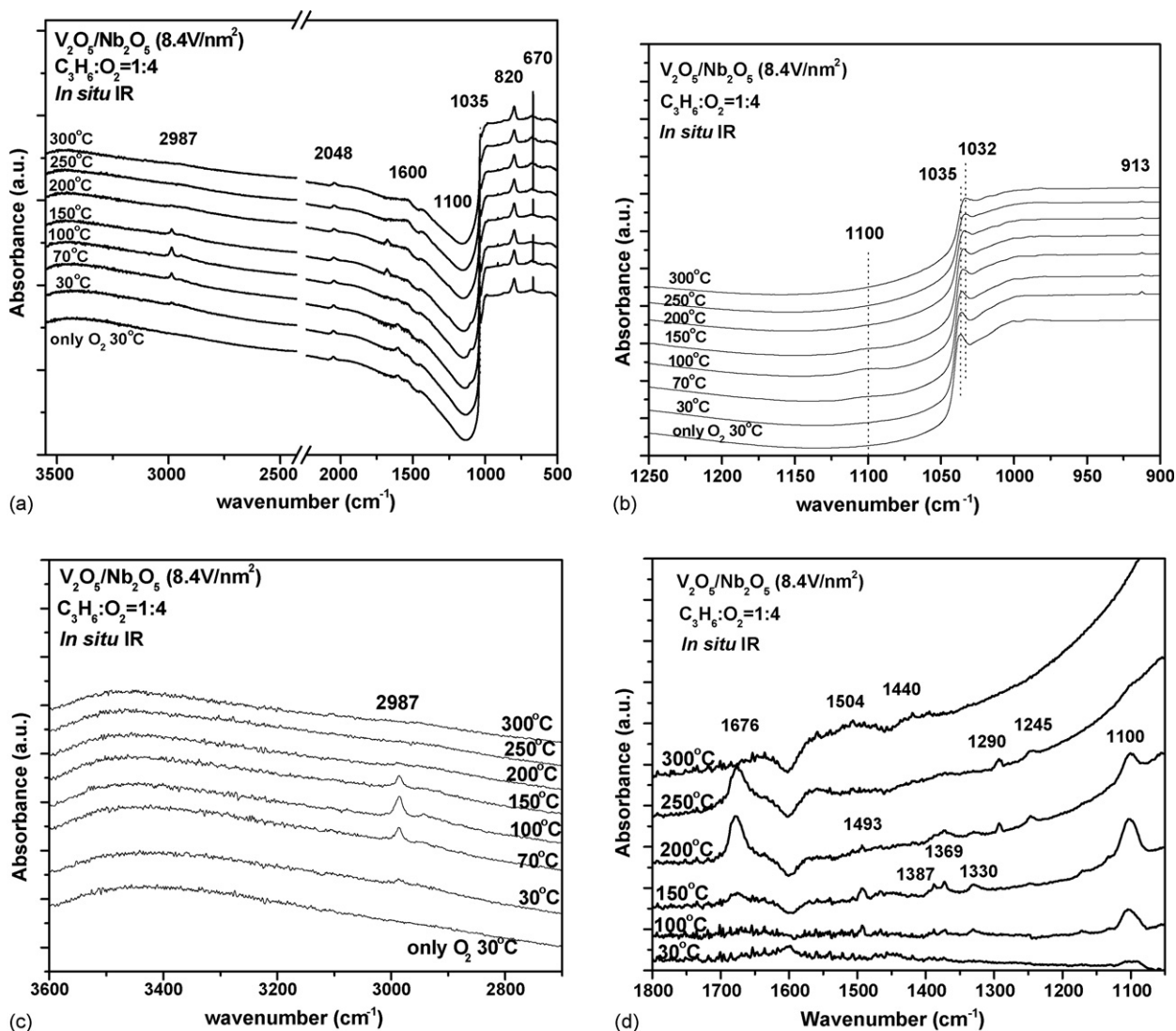

Fig. 3. *In situ* infrared spectra, in the: (a) 500–3600 cm^{-1}, (b) 900–1350 cm^{-1}, (c) 2700–3600 cm^{-1} range, (d) *In situ* difference infrared spectra, in the 1050–1800 cm^{-1} range, of supported V_2O_5/Nb_2O_5 (8.4 V/nm) during propylene oxidation (C_3H_6:O_2 = 1:4) as a function of catalyst temperature.

changes taking place with the surface reaction intermediates during the propylene oxidation reaction. Adsorption of propylene at room temperature leads to formation of two new broad bands at 1607 and 1100 cm^{-1} that have been assigned to σ-bonded and π-bonded chemisorbed propylene [54,55]. Upon increasing the catalyst reaction temperature, the weak 1607 cm^{-1} IR band due to adsorbed σ-bonded propylene is not present at 100 °C. At higher temperatures, the negative IR features at ~1600 cm^{-1} are a consequence of the lower amount of physisorbed moisture under reaction conditions compared to the dehydrated catalyst. This is a related to the more strongly bound surface reaction intermediates compared to physisorbed moisture, and, consequently, the reaction intermediates are displacing moisture from the catalyst surface under reaction conditions. Simultaneously, as the reaction temperature is increased, the 1100 cm^{-1} IR band from the adsorbed π-bonded propylene increases in intensity. The maximum intensity of the adsorbed π-bonded propylene is observed at 150 °C and the π-bonded propylene is not present at 250 °C and higher catalytic reaction temperatures. New IR bands appear at 1330, 1369, 1387, and 1493 cm^{-1} in the 100–250 °C temperature range and have previously been assigned to surface allyl intermediates [54]. The weak 1493 cm^{-1} IR band is associated with the C–C vibrations of the symmetric π-allyl species (CH2–CH*–CH2, where the * asterisk represents a catalyst surface site) [54]. The weak IR bands at 1329, 1369 and 1384 cm^{-1} are associated with the δ_{CH_2} bending modes of π-allyl species [56]. The IR vibrations of the surface π-allyl species disappear at 200 °C and new IR bands at 1245, 1290 and 1673 cm^{-1} appear. The strong IR band at 1673 cm^{-1}, as well as weak bands 1245 and 1290 cm^{-1}, are characterized of σ-allyl species (*CH2–CH=CH2) [57] and are no longer present in the IR spectrum at 300 °C. At 300 °C new weak and broad bands appear at 1504 and 1440 cm^{-1} that are most probably from propylene decomposition species such as acetic acid [54,58,59]. The IR band for the carbonyl vibrations of adsorbed acrolein appear at 1662 and 1700 cm^{-1} [60], however, are not present at any temperature during propylene oxidation. Thus, the surface σ-allyl (*CH2–CH–CH2) species is the *most abundant reaction intermediate* (mari) during the selective oxidation of propylene above ~200 °C over the supported V_2O_5/Nb_2O_5 monolayer catalyst.

The *in situ* IR spectra of the supported V_2O_5/Nb_2O_5 (8.4 V/nm^2) catalyst were also collected in an O_2-free C_3H_6/He environment at different temperatures. In the O_2-free C_3H_6 environment, however, none of the IR bands associated with the surface allyl species were present. Thus, the formation of surface allyl intermediates during propylene adsorption on supported VO_x/Nb_2O_5 catalysts appears to be dependent on the presence of gaseous molecular O_2.

3.4. C_3H_6-temperature programmed surface reaction spectroscopy

C_3H_6-TPSR spectroscopy experiments were undertaken with the supported VO_x/Nb_2O_5 catalyst (8.4 V/nm^2) to investigate the catalytic surface reaction mechanism of propylene oxidation to acrolein. The O_2-free C_3H_6-TPSR spectra are shown in Fig. 4a
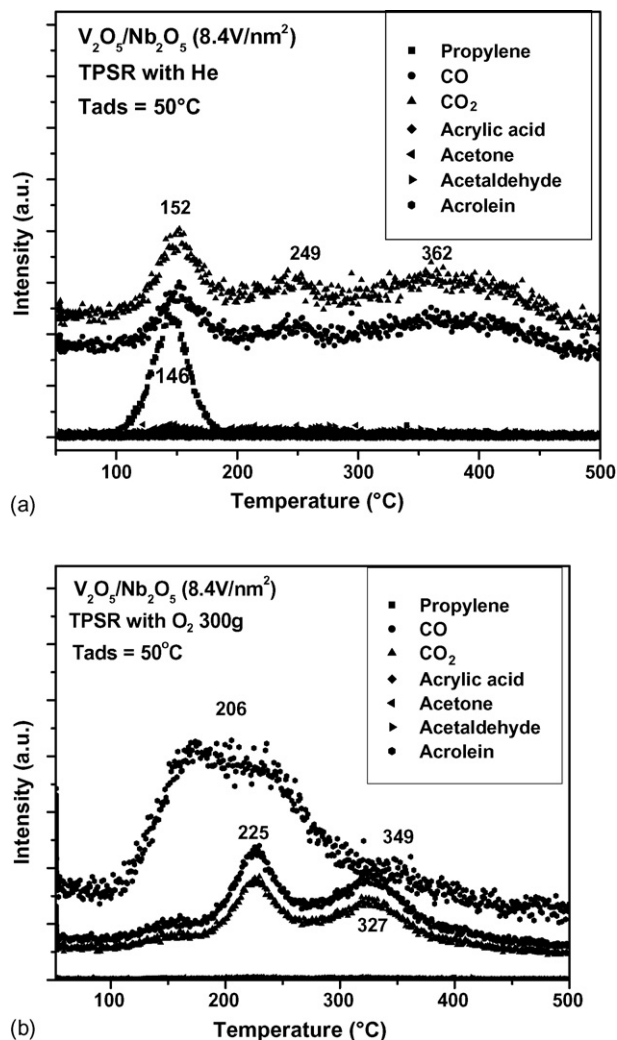

Fig. 4. (a) C_3H_6-TPSR spectra in flowing He (O_2-free). (b) C_3H_6-TPSR spectra in flowing O_2/He.

and the main reaction products from propylene oxidation by the lattice oxygen from the surface vanadia species are CO/CO_2. The CO and CO_2 appear in three different temperature ranges with T_p values of 152, 249 and 361 °C. No C_3-oxygenated products (acrolein, acrylic acid or acetone) were detected. Chemisorbed propylene desorbed at $T_p \sim 146$ °C and cannot be related to physically adsorbed propylene that desorbs at significantly lower temperatures [61]. These C_3H_6-TPSR findings reveal that the surface lattice oxygen from the surface vanadia species is not able to activate propylene and selective oxidize propylene to acrolein. In the presence of gaseous molecular O_2, however, the C_3H_6-TPSR experiment yields acrolein as the main reaction product in two different temperature regions as shown in Fig. 4b. The acrolein T_p values are 206 and 349 °C, with most of the acrolein forming at the lower temperature range. Interestingly, the formation of CO/CO_2 at ~150 °C is suppressed in the presence of gas phase O_2 and CO/CO_2 production primarily occurs with T_p values of 225 and 327 °C. The presence of gas phase O_2 appears to retard the kinetics of CO/CO_2 formation during propylene oxidation. The desorption of unreacted propylene is not detected in the presence of molecular O_2 and further indicates that the

presence of gaseous molecular O_2 is critical for activating propylene to acrolein. Thus, the selective oxidation of propylene to acrolein over the supported vanadia catalysts follows a Langmuir–Hinshelwood reaction mechanism where both reactants must be present and chemisorbed on the catalyst surface for this selective oxidation pathway to take place.

The surface kinetics for the rds of selective propylene oxidation to acrolein was determined by applying the Redhead Eq. [40]. It was assumed that the rds reaction step was first-order and that the first-order pre-exponential factor was 10^{13} s^{-1}. For the acrolein T_p value of 206 °C and the heating rate of 10 °C/min, the activation energy of 32.7 kcal/mol was determined from application of the Redhead equation.

3.5. Steady-state propylene oxidation to acrolein

3.5.1. Product selectivity for propylene oxidation over supported V_2O_5/Nb_2O_5 catalysts

The steady-state findings for the selective oxidation of propylene over the supported V_2O_5/Nb_2O_5 catalysts are presented in Table 2. The product selectivity for propylene oxidation over the supported V_2O_5/Nb_2O_5 catalysts at 300 °C is presented in Fig. 5 as a function of surface vanadia coverage. The main reaction product from propylene oxidation over the supported vanadia-niobia catalysts is acrolein with smaller amounts of acetone, CO, CO_2, acrylic acid and C_2 products (acetic acid, acetaldehyde and ethylene). The acrolein selectivity increases from 50 to 91% with surface vanadia coverage in the sub-monolayer region. The strong increase in acrolein selectivity and strong decrease in byproducts with surface vanadia coverage
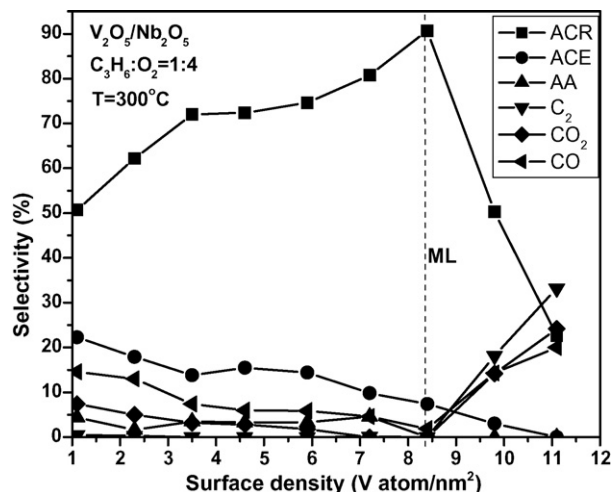

Fig. 5. Product selectivity from propylene oxidation over supported V_2O_5/Nb_2O_5 catalysts as a function of vanadia loading (V/nm²).

on the Nb_2O_5 support reveals that exposed Nb cationic sites are not selective for acrolein formation. Consequently, the highest acrolein selectivity corresponds to monolayer surface vanadia coverage where all the exposed support Nb cations are covered by the two-dimensional surface vanadia phase. The major non-acrolein product is acetone, and its selectivity monotonically decreases with increasing surface vanadia coverage in the sub-monolayer range (see Fig. 5). For the monolayer supported V_2O_5/Nb_2O_5 catalyst, 8.4 V/nm², varying the C_3H_6/O_2 ratio essentially does not influence the reaction selectivity as shown by the data in Table 3. Above monolayer surface vanadia coverage, crystalline V_2O_5 nanoparticles are also present (see Raman section above),

Table 2

Catalytic results of propylene oxidation over supported V_2O_5/Nb_2O_5 catalysts at 300 °C

V_2O_5/Nb_2O_5 surface density (V/nm²)	Conversion (%)	Act_{acr} [a] (mmol/g h)	TOF_{acr} [b] (10^{-3} S^{-1})	Selectivity [c] (%)					
				Acr	Ace	AA	CO	CO_2	C_2
1.1	0.06	0.2	0.5	51	22	4	1	7	15
2.3	0.17	0.7	0.8	62	18	2	0	5	13
3.5	0.30	1.4	1.2	72	14	4	0	3	7
4.7	0.75	3.5	2.0	72	16	3	0	3	6
5.9	1.13	5.5	2.8	75	14	3	0	2	6
7.2	1.80	9.5	4.1	81	10	5	0	0	5
8.4 [d]	2.38	14.2	5.0	91	7	0	1	0	1
9.8	0.92	3.0	–	50	3	0	15	14	18
11.1	0.10	0.1	–	23	0	0	24	20	33

$C_3H_6:O_2: He = 1:4:5$, total flow rate 50 cm³/min.
[a] Millimoles of acrolein formed per gram catalyst per hour.
[b] TOF is calculated on the basis of the V atoms in the catalysts for propylene converted to acrolein.
[c] Acr: acrolein, AA: acrylic acid, ACE: acetone, C_2: ethylene, acetice acid, acetaldehyde.
[d] Surface monolayer coverage.

Table 3

Effect of gas-phase C_3H_6/O_2 ratio on propylene oxidation TOF and selectivity for the supported V_2O_5/Nb_2O_5 (8.4 V/nm²) catalyst at 300 °C

Condition	TOF (10^{-3} s^{-1})	Conversion (%)	Selectivity Acr (%)	Ace (%)	AA (%)	C_2 (%)	CO_2 (%)	CO (%)
$C_3H_6:O_2 = 1:4$	4.5	2.03	91	7	0	1	0	1
$C_3H_6:O_2 = 1:2$	4.5	2.01	88	8	0	2	0	2
$C_3H_6:O_2 = 1:1$	4.4	1.93	90	8	0	0	0	2
$C_3H_6:O_2 = 2:1$	3.9	1.78	90	7	0	1	0	2

the catalytic activity decreases and the acrolein selectivity dramatically drops with the cracked $C_2/CO/CO_2$ product selectivity dramatically increasing with increasing content of crystalline V_2O_5 nanoparticles in the catalyst. Thus, the surface vanadia species on Nb_2O_5 are the catalytic active sites for selective oxidation of propylene to acrolein and the surface vanadia coverage on the Nb_2O_5 support has the most significant effect on this partial oxidation reaction.

3.5.2. Number of catalytic active sites participating in the rate-determining-step

The number of catalytic active surface VO_x sites/g increases linearly with vanadia loading in the sub-monolayer region where the vanadia is 100% dispersed on the Nb_2O_5 support. This linear relationship allows for the quantitative determination of the number of surface catalytic active sites involved in the kinetic rate-determining-step of propylene oxidation to acrolein. The kinetic expression for the rate of propylene oxidation to acrolein can be expressed as a power law:

$$r = k[C_3H_6]^x[O_2]^y[N_s]^n \tag{1}$$

where r represents the rate of reaction to acrolein (mmol acrolein/(g h)), N_s is the number of surface vanadia sites/g, k is the Arrhenius rate constant, x and y represent the reactant reaction orders (determined below), and the exponent n represents the number of catalytic sites involved in the rate-determining-step of the propylene oxidation to acrolein reaction. For constant partial pressures of the reactants, temperature, and flow rates, Eq. (1) can be further simplified as

$$r = k'[N_s]^n, \tag{2}$$

where k' includes all the constant parameters (k, $[C_3^=]^x$ and $[O_2]^y$). The exponent n represents the number of catalytic active surface VO_x sites involved in the rds. The exponent n can be readily determined from the slope of the plot log activity (mmol acrolein/(g h)) versus log N_s (V/g) and this plot is depicted in Fig. 6. For propylene oxidation to acrolein over the supported
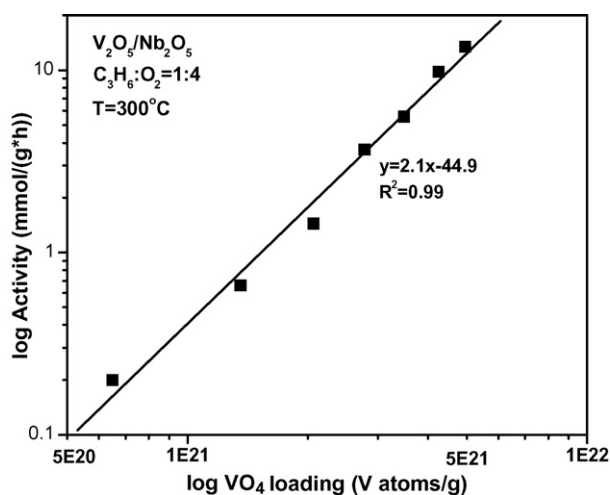
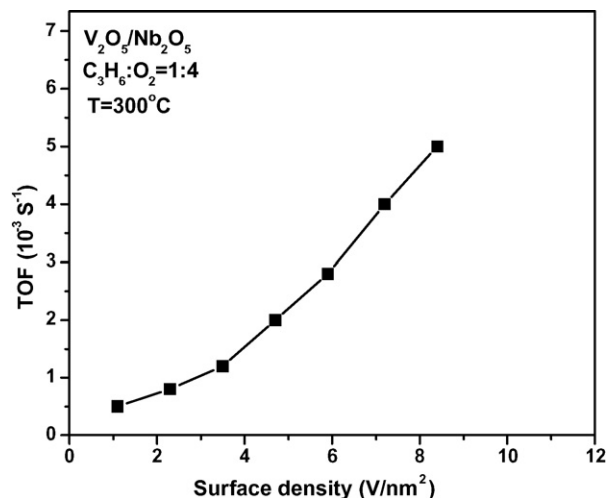Fig. 6. Plot of log activity (mmol/g h) vs. log N_s (V/g) for $T = 300\ °C$ and $C_3H_6:O_2 = 1:4$.

Fig. 7. Acrolein formation TOF (s^{-1}) over supported V_2O_5/Nb_2O_5 catalysts as a function of vanadia loading (V/nm^2).

vanadia catalysts, the slope has a value of ∼2 indicating that two surface VO_x sites are involved in the rds of this selective oxidation reaction.

As already mentioned, the TOF for propylene oxidation to acrolein over the supported V_2O_5/Nb_2O_5 catalysts can be quantitatively determined for catalysts in the sub-monolayer surface coverage range where all the catalytic active surface vanadia sites are exposed to the reactants (see Fig. 7). The acrolein TOF is strongly dependent on the surface vanadia coverage and increases from 0.48×10^{-3} to $5.0 \times 10^{-3}\ s^{-1}$. Note that this more than a factor of 10 increase in TOF is not affected by the increase in selectivity with surface vanadia coverage since the corresponding selectivity increase varies by less than a factor of 2 (see Figs. 5 and 7).

3.5.3. Reaction orders for C_3H_6 and O_2

Propylene oxidation to acrolein over the supported V_2O_5/Nb_2O_5 catalysts is strongly dependent on both the propylene and oxygen partial pressures as shown by the catalytic activity data in Fig. 8a and b. These plots reveal that the propylene oxidation to acrolein reaction follows around first-order kinetics with respect to C_3H_6 and around half-order kinetics with respect to molecular O_2 partial pressures. Furthermore, the dependence of propylene oxidation to acrolein over the supported V_2O_5/Nb_2O_5 catalysts on both the C_3H_6 and O_2 partial pressures reveals that this reaction follows Langmuir–Hinshelwood kinetics and is in agreement with the C_3H_6-TPSR findings above [62].

3.5.4. Apparent activation energy for propylene oxidation to acrolein

The apparent activation energy, E_{app}, for propylene oxidation to acrolein over the supported VO_x/Nb_2O_5 catalyst containing monolayer surface vanadia coverage (8.4 V/nm^2) was determined from the plot of ln(TOF$_{acr}$) versus $1/T$ shown below in Fig. 9. A linear relationship was obtained with the apparent activation energy of 15.4 kcal/mol. This value for E_{app}
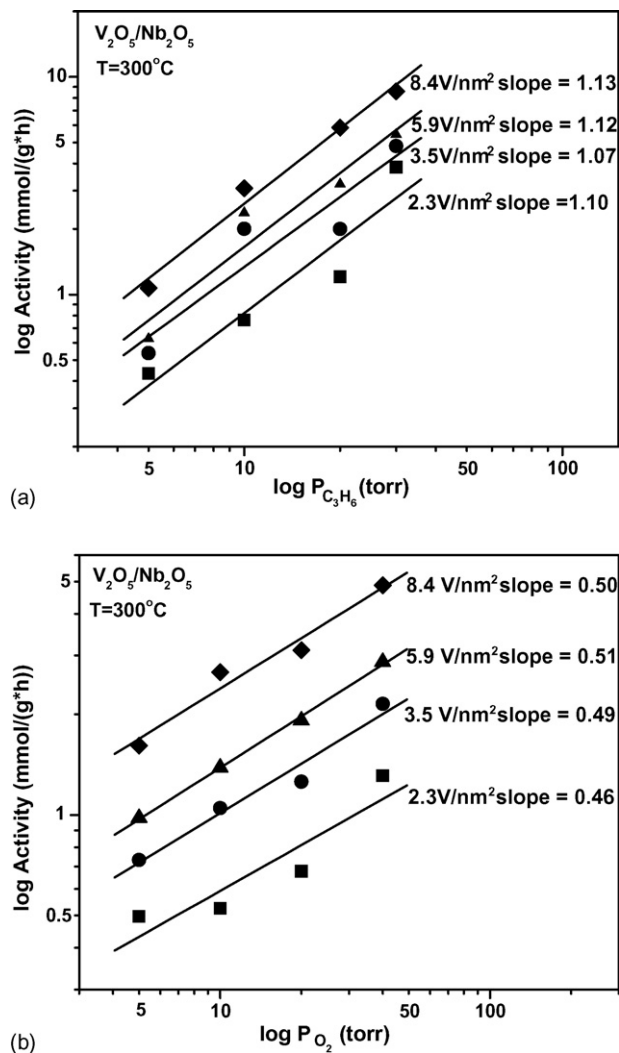
Fig. 8. (a) Dependence of propylene oxidation to acrolein kinetics on the propylene partial pressure. (b) Dependence of propylene oxidation to acrolein kinetics on the gas phase molecular O_2 partial pressure.
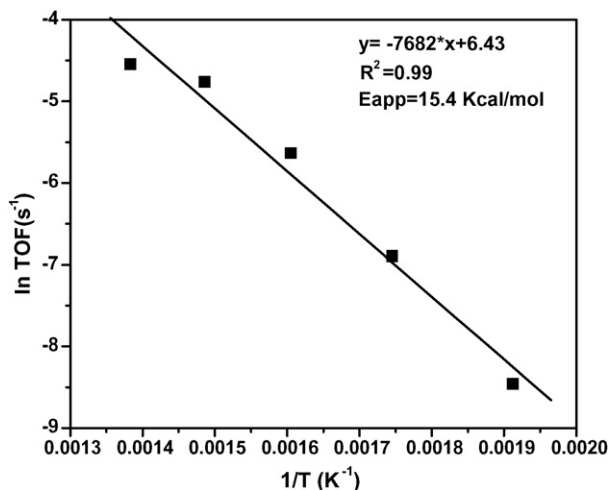

Fig. 9. ln(TOF) vs. $1/T$ (K^{-1}) plot for determination of E_{act} for propylene oxidation to acrolein over supported V_2O_5/Nb_2O_5 (8.4 V/nm^2) catalyst.

is similar to that found for propylene oxidation over bulk Bi_2MoO_6 catalysts (15–20 kcal/mol above 400 °C) [4,19]. The surface activation energy (E_{act}) was estimated above from the Redhead equation, which allows determination of the apparent heat of adsorption for propylene on the supported V_2O_5/Nb_2O_5 monolayer surface vanadia catalyst from the well known relationship:

$$E_{app} = E_{act} + \Delta H_{ads}. \tag{3}$$

where ΔH_{ads} is the heat of propylene adsorption. From Eq. (3), an apparent propylene heat of adsorption of 17.3 kcal/mol is obtained. This value for the heat of adsorption of propylene on supported V_2O_5/Nb_2O_5 is in line with the range of heat of adsorption values, 13–28 kcal/mol, determined for Bi_2O_3-MoO_3 catalysts as a function of propylene surface coverage [63].
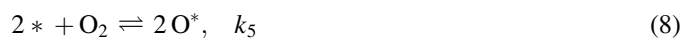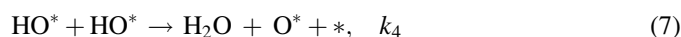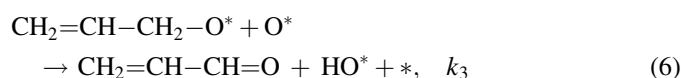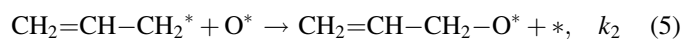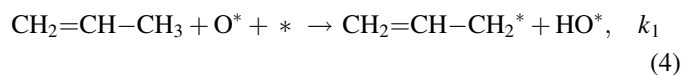
4. Discussion

The *in situ* Raman spectra of the dehydrated supported V_2O_5/Nb_2O_5 catalyst revealed that the supported vanadia phase is present as isolated surface VO_x species, polymerized surface VO_x species, and crystalline V_2O_5 nanoparticles. The V_2O_5 nanoparticles are only present above monolayer surface vanadia coverage. The extent of polymerization of the surface VO_x species cannot be quantitatively determined for the supported V_2O_5/Nb_2O_5 catalyst because of the strong UV–vis absorption by the Nb_2O_5 support in the vanadia region [39]. The shift in the terminal V=O vibration from 1028 to 1035 cm^{-1} with surface vanadia coverage, however, reflects the polymerization of the surface vanadia species on the Nb_2O_5 support [48].

The surface vanadia species also become partially reduced during propylene oxidation to acrolein and the reduction extent increases with the gas phase C_3H_6/O_2 ratio. Only the fully oxidized surface vanadia species, however, are able to provide the needed oxygen for the propylene oxidation reaction by becoming reduced from V^{5+} to V^{4+}/V^{3+} species upon releasing the oxygen [64]. Re-oxidation of the reduced surface vanadia species by molecular O_2 might proceed by the formation of superoxide and peroxide O_2 species, however, neither surface superoxide, $\sim$1125 cm^{-1}, or surface peroxide, $\sim$830–870 cm^{-1} molecular O_2 species are found to be present on the catalyst surface during steady-state selective oxidation of propylene to acrolein [65]. This suggests that such re-oxidation reactions are extremely rapid or that such chemisorbed molecular O_2 oxide structures are thermally unstable under reaction conditions with extremely short lifetimes. Furthermore, the half-order dependence on the O_2 partial pressure during propylene oxidation to acrolein is consistent with an atomic form of chemisorbed oxygen, rather than molecular O_2, participating in the rds.

The *in situ* IR measurements of the supported V_2O_5/Nb_2O_5 monolayer catalyst revealed that surface allyl species were the most abundant reaction intermediates (mari) on the catalyst surface during propylene oxidation to acrolein. Furthermore,

the surface σ-allyl (*CH$_2$–CH=CH$_2$) intermediate was the predominant surface allylic species on the catalyst for reaction temperatures of ∼200–300 °C. Both the *in situ* IR and C$_3$H$_6$-TPSR studies demonstrated that the surface allyl intermediates and acrolein formation, respectively, required the presence of gas-phase oxygen for their formation. This suggests that the surface VO$_x$ catalytic active sites need to be maintained in the fully oxidized V^{5+} state for selective oxidation of propylene to acrolein.

In addition, to these molecular spectroscopic insights, the steady-state reaction kinetics for selective oxidation of propylene to acrolein exhibit first-order dependence on the partial pressure of propylene and half-order dependence on the partial pressure of molecular O$_2$. As already mentioned above, surface molecular O$_2$ species were not detected during propylene oxidation and the half-order kinetic dependence on the oxygen partial pressure is only consistent with the participation of dissociated chemisorbed atomic oxygen. The first-order dependence of the reaction kinetics on propylene partial pressure reflects the participation of a C$_3$H$_x$ unit in the rds of propylene oxidation to acrolein. Lastly, variation of the surface VO$_x$ density in the sub-monolayer region revealed that two surface VO$_x$ units are involved in the selective oxidation of propylene to acrolein. One surface VO$_x$ unit is required to abstract the two H atoms from the terminal methyl group of the propylene molecule and a second VO$_x$ unit is required to insert an O atom to yield acrolein. From these fundamental molecular insights, the following reaction mechanism is proposed for the selective oxidation of propylene to acrolein over the supported V$_2$O$_5$/Nb$_2$O$_5$ catalysts:

$$CH_2{=}CH{-}CH_3 + O^* + {*} \rightarrow CH_2{=}CH{-}CH_2{}^* + HO^*, \quad k_1 \tag{4}$$

$$CH_2{=}CH{-}CH_2{}^* + O^* \rightarrow CH_2{=}CH{-}CH_2{-}O^* + {*}, \quad k_2 \tag{5}$$

$$CH_2{=}CH{-}CH_2{-}O^* + O^* \rightarrow CH_2{=}CH{-}CH{=}O + HO^* + {*}, \quad k_3 \tag{6}$$

$$HO^* + HO^* \rightarrow H_2O + O^* + {*}, \quad k_4 \tag{7}$$

$$2\,{*} + O_2 \rightleftharpoons 2\,O^*, \quad k_5 \tag{8}$$

The first step in the selective oxidation of propylene to acrolein is the formation of a surface allyl species by abstraction of a methyl H (Eq. (4)), which is consistent with the reaction mechanisms previously proposed by Grasselli and Keulks' [2,4,5,8]. The subsequent reaction step is the insertion of the O atom to form the σ-allyl-O* surface species (Eq. (5)). The expulsion of the second H from the oxygen end of the surface CH$_2$=CH–CH$_2$–O* intermediate is either a concerted reaction that occurs simultaneously with O insertion or quickly in a subsequent reaction step (Eq. (6)). The surface hydroxyl species formed during the two H abstraction reaction steps rapidly recombine to form H$_2$O (Eq. (7)). Lastly, the reduced surface vanadia sites are re-oxidized by gas phase molecular oxygen (Eq. (8)). Furthermore, the selective oxidation of propylene to acrolein will not proceed in the absence of gas phase molecular O$_2$, which suggests that the surface vanadia species must be maintained in its fully oxidized state during reaction. The need for gaseous molecular O$_2$ for the selective oxidation of propylene to acrolein over the supported V$_2$O$_5$/Nb$_2$O$_5$ catalytic system also underscores the Langmuir–Hinshelwood reaction mechanism of this catalytic system.

Many investigations have proposed that the rate-determining-step (rds) in the selective oxidation of propylene over bulk mixed metal oxide catalysts involves breaking of the methyl C–H bond in the CH$_2$=CHCH$_3$ molecule [2,4,5,8,66,67]. Application of the steady-state approximation to the propylene oxidation kinetics results in the same general kinetic expression, first-order in propylene and half-order in O$_2$, if either of reaction steps 2, 3 or 4 (Eqs. (5)–(7)) are assumed to be the rds. The chemisorption of gaseous propylene cannot be the rds for propylene oxidation over supported V$_2$O$_5$/Nb$_2$O$_5$ since the C$_3$H$_6$-TPSR experiment reveals that propylene chemisorption readily occurs at 50 °C and that the formation of acrolein occurs ∼200 °C. Thus, the rds step in propylene oxidation to acrolein over supported V$_2$O$_5$/Nb$_2$O$_5$ catalysts must involve either (i) oxygen insertion into the surface allyl intermediate, step 2 (Eq. (5)), (ii) C–H bond breaking to form the surface allyl intermediate, step 1 (Eq. (4)) or may even occur in one step if the breaking of the surface allyl C–H bond is in concert with the insertion of the O surface atom. Studies with the isotopes C$_3$D$_6$ and ^{18}O$_2$ will be required to fully determine the rds for the selective oxidation of propylene to acrolein and will be reported in the future.

The surface VO$_x$ species on the Nb$_2$O$_5$ support possess three different types of oxygen functionalities: terminal V=O (∼1030 cm^{-1}), bridging V–O–Nb (∼940 cm^{-1}) and bridging V–O–V. For the supported V$_2$O$_5$/Nb$_2$O$_5$ catalyst system, it is not possible to directly detect the bridging V–O–V vibrations because of the strong Nb$_2$O$_5$ vibrations below 800 cm^{-1}. The shift of the terminal V=O vibration with surface vanadia coverage, however, is a consequence of the distortions of the surface VO$_x$ species induced by the formation of bridging V–O–V bonds as the surface VO$_x$ units polymerize [48]. The terminal V=O bond is not involved in the rds because the terminal V=O bond vibration is constant at 1035 cm^{-1} for 5.9–8.4 V/nm^2 and at 1028 cm^{-1} for 2.3–3.5 V/nm^2, but the corresponding TOF values increase by a factor of ∼1.5–2 for these two sets of supported V$_2$O$_5$/Nb$_2$O$_5$ catalysts (see Fig. 7). Increasing the surface vanadia coverage increases both the concentration of bridging V–O–V bonds and the corresponding TOF for acrolein formation. At first glance, these two parameters appear to correlate, but catalytic oxidation studies with other chemical probe molecules over the same catalysts do not exhibit a change in the TOF value as a function of surface vanadia coverage. The propane to propylene [68] and CH$_3$OH to H$_2$CO [42] catalytic oxidative dehydrogenation reactions exhibit constant TOF values with surface vanadia coverage because these reactions only require one surface VO$_x$ unit or oxygen atom to remove the two hydrogen atoms as water. In contrast, propylene oxidation to acrolein kinetics reveal that two surface VO$_x$ units (see Fig. 6) are required since this reaction requires two O atoms: one O atom to remove the two H atoms as

water and a second O atom to insert into the C_3H_x intermediate. As a result, the apparent increase in acrolein TOF with surface vanadia coverage is not related to a greater TOF value for the polymeric surface vanadia species relative to the isolated surface vanadia species, but is strictly a consequence of the requirement for the participation of two surface VO_x sites in this oxidation reaction. Note that the concentration of two surface VO_x species for the supported V_2O_5/Nb_2O_5 catalyst system varies as $[VO_x]^2$ below monolayer surface coverage. Examining the catalytic role of the bridging V–O–Nb bond upon the selective oxidation of propylene to acrolein requires investigating the influence of other support cations. Such studies have already been undertaken and also demonstrate that the TOF for acrolein formation varies by two orders of magnitude as the specific oxide support is varied ($TiO_2 > ZrO_2 > Nb_2O_5 > Al_2O_3 > SiO_2$) [69]. Thus, it appears that the oxygen functionality involved in the selective propylene oxidation to acrolein rds is the bridging V–O–Nb bond.

The acrolein selectivity during propylene oxidation over the supported vanadia catalysts was found to significantly increase with surface vanadia coverage with the main byproduct being acetone (see Fig. 5). It has been proposed that acetone formation proceeds by reaction of π-bonded surface allylic species with surface Bronsted acid sites that form surface isoproxide species that subsequently dehydrogenate to acetone [56,57]. The calcined Nb_2O_5 support does not possess surface Bronsted acid sites and only exhibits modest surface Lewis acid sites [70]. At low surface vanadia coverage, the isolated surface vanadia species usually do not exhibit Bronsted acidity [71]. Nevertheless, it appears that the formation of the acetone byproduct is mainly related to the exposed Lewis acid surface Nb sites from the Nb_2O_5 support in the sub-monolayer region. Some residual acetone still forms at monolayer surface vanadia coverage and this may have its origin in the surface Bronsted acid sites associated with the polymeric surface vanadia species present at high surface vanadia coverage [72].

5. Conclusions

The supported V_2O_5/Nb_2O_5 catalysts contain three different vanadia structures whose relative concentration depends on surface vanadia coverage. At low surface vanadia coverage, the vanadia species are present as isolated surface VO_x units. At intermediate surface vanadia coverage, both isolated and polymeric surface VO_x units coexist. Above monolayer surface vanadia coverage (>8.4 V/nm^2), crystalline V_2O_5 nanoparticles are also present on top of the surface VO_x monolayer. The surface VO_x species attached to the Nb_2O_5 support are the catalytic active sites for selective oxidation of propylene to acrolein and the crystalline V_2O_5 nanoparticles are not selective for this partial oxidation reaction. The propylene oxidation reaction proceeds via surface allyl species with the rate-determining-step involving either C–H bond breaking or oxygen insertion. This reaction requires the participation of two oxygen atoms that are supplied by two surface VO_x sites. The reaction proceeds via a Langmuir–Hinshelwood mechanism since its rate varies as first-order with the propylene partial pressure and half-order with the molecular O_2 partial pressure.

The activation of propylene to surface allyl intermediates and the presence of fully oxidized surface VO_x requires the presence of gas phase molecular O_2. The critical oxygen participating in this selective oxidation reaction is the oxygen functionality of the bridging V–O–Nb bond. The highest acrolein selectivity corresponds to the monolayer surface vanadia catalyst since the monolayer covers the underlying surface Nb Lewis acid sites of the Nb_2O_5 support that are associated with acetone byproduct formation.

References

[1] R.K. Grasselli, in: G. Ertl, H. Knoezinger, J. Weitkamp (Eds.), Handbook of Heterogeneous Catalysis, vol. 5, VCH verlagsgesellschaft mbH, Weinheim, Federal Republic of Germany, 1997, p. 2303.
[2] R.K. Grasselli, Top. Catal. 21 (2002) 79.
[3] C.R. Adams, H.H. Voge, C.Z. Morgan, W.E. Armstrong, J. Catal. 3 (1964) 379.
[4] D. Krenzke, G.W. Keulks, J. Catal. 64 (1980) 295.
[5] G.W. Keulks, J. Catal. 19 (1970) 232.
[6] J.M. Lieto, R. Bielsa, G. Kremenic, J.L. Fierro, Stud. Surf. Sci. Catal. 55 (1990) 295.
[7] Y. Moro-oka, W. Ueda, Adv. Catal. 40 (1995) 233.
[8] R.K. Grasselli, G. Centi, F. Trifiro, Appl. Catal. 57 (1990) 149.
[9] M. Allen, R. Betteley, M. Bowker, G.J. Hutching, Catal. Today 9 (1991) 97.
[10] G.W. Godin, C.C. MacCain, E.A. S Porter, in: Proceedings of Fourth International Congress of Catalysis vol. 1, Adler, New York, 1968, p. 271.
[11] M. Carbucicchio, G. Centi, P. Forzatti, F. Trifiro, P.L. Villa, J. Catal. 107 (1987) 307.
[12] D. He, W. Ueda, Y. Moro-oka, Catal. Lett. 12 (1992) 35.
[13] K.H. Schultz, D.F. Cox, J. Catal. 143 (1993) 464.
[14] A.N. Desikan, W. Zhang, S.T. Oyama, J. Catal. 157 (1995) 740.
[15] C. Doornkamp, V. Ponec, J. Mol. Catal. A: Chem. 162 (2000) 19.
[16] M.M. Bettahar, G. Constentin, L. Savary, J.C. Lavalley, Appl. Catal. A 145 (1996) 1.
[17] A. Bielanski, J. Haber, in: M. Dekker (Ed.), Oxygen in Catalysis, Wiley, New York, 1991, p. 231.
[18] R.K. Grasselli, Catal. Today 49 (1999) 141.
[19] J.R. Monnier, G.W. Keulks, J. Catal. 68 (1981) 51.
[20] E.M. Al'kaeva, T.V. Andrushkevich, O.Yu. Ovsitser, V.D. Sokolovskii, Catal. Today 24 (1995) 357.
[21] J.R. Monnier, G.W. Keulks, J. Catal. 68 (1981) 51.
[22] R.K. Grasselli, J.D. Burrington, Adv. Catal. 30 (1981) 133.
[23] N. Arora, G. Deo, I.E. Wachs, A.M. Hirt, J. Catal. 159 (1995) 1.
[24] J. Holmberg, R.K. Grasselli, A. Andersson, Appl. Catal. A 270 (2004) 121.
[25] R.K. Grasselli, D.J. Buttrey, P. DeSanto, J.D. Burrington, Catal. Today 91 (2004) 251.
[26] W. Ueda, Y. Moro-oka, T. Ikawa, J. Catal. 88 (1984) 214.
[27] R.K. Grasselli, J.D. Burrington, D.J. Buttrey, P. De Santo, C.G. Lugmair, A.F. Volpe, T. Weingand, Top. Catal. 23 (2003) 1.
[28] W. Ueda, D. Vitry, T. Katou, Catal. Today 99 (2005) 43.
[29] Z. Zhao, X. Gao, I.E. Wachs, J. Phys. Chem. B 107 (2003) 6333.
[30] D. Vitry, J. Dubois, W. Ueda, J. Mol. Catal. A: Chem. 220 (2004) 67.
[31] I.E. Wachs, Catal. Today 100 (2005) 79.

[32] L. Burcham, G. Deo, X. Gao, I.E. Wachs, Top. Catal. 11 (2000) 85.

[33] S. Xie, E. Iglesia, A.T. Bell, Langmuir 16 (2000) 7162.

[34] H. Dai, A.T. Bell, E. Iglesia, J. Catal. 221 (2004) 491.

[35] A. Khodakov, B. Olthof, A.T. Bell, E. Iglesia, J. Catal. 181 (1999) 205.

[36] L. Burcham, M. Badlani, I.E. Wachs, J. Catal. 203 (2001) 104.

[37] X. Gao, I.E. Wachs, Top. Catal. 18 (2002) 243.

[38] X. Gao, S. Bare, B.M. Weckhuysen, I.E. Wachs, J. Phys. Chem. B 102 (1998) 10842.

[39] X. Gao, I.E. Wachs, J. Phys. Chem. 104 (2000) 1261.

[40] P.A. Redhead, Vacuum 12 (1962) 213.

[41] I.E. Wachs, Catal. Today 27 (1996) 437.

[42] G. Deo, I.E. Wachs, J. Catal. 146 (1994) 323.

[43] I.E. Wachs, B.M. Weckhuysen, Appl. Catal. A: Gen. 157 (1997) 67.

[44] G. Busca, J. Raman Spectrosc. 33 (2002) 348.

[45] J.M. Jehng, J. Phys. Chem. B 104 (1998) 462.

[46] G. Xiong, V.S. Sullivan, P.C. Stair, G.W. Zajac, S.S. Trail, J.A. Kaduk, J.T. Golab, J.F. Brazdil, J. Catal. 230 (2005) 317.

[47] Z. Wu, H. Hack-Sung, P. Stair, S. Rugmini, S.D. Jackson, J. Phys. Chem. B 109 (2005) 2793.

[48] H. Tian, E. Ross, I.E. Wachs, J. Phys. Chem. B 110 (2006) 9593.

[49] A. Khodakov, B. Olthof, A.T. Bell, E. Iglesia, J. Catal. 181 (1999) 205.

[50] M. Ristic, S. Popovic, S. Music, Mat. Lett. 58 (2004) 2658.

[51] W. Chen, Y. Kaneko, N. Kinomura, J. Appl. Electrochem. 32 (2003) 515.

[52] C. Resini, T. Montanari, G. Busca, J.-M. Jehng, I.E. Wachs, Catal. Today 99 (2005) 105.

[53] A.L. Smith, The Coblentz Society Desk Book of Infrared Spectra, second ed., Coblentz Society, Kirkwood, 1982, p. 1.

[54] P. Concepcion, P. Botella, J.M. Lopez Nieto, Appl. Catal. A 278 (2004) 45.

[55] V.S. Sanchez Escribano, G. Busca, V. Lorenzelli, J. Phys. Chem. 94 (1990) 8939.

[56] E.B. Burgina, E.N. Yurchenko, J. Mol. Struct. 116 (1984) 17.

[57] A.A. Davydov, V.G. Mikhaltchenko, V.D. Sokolovskii, G.K. Boreskov, J. Catal. 55 (1978) 299.

[58] V.S. Escribano, G. Busca, V. Lorenzelli, J. Phys. Chem. 94 (1990) 8939.

[59] V. Ermini, E. Finocchio, S. Sechi, G. Busca, S. Rossini, Appl. Catal. A: Gen. 190 (2000) 157.

[60] J.C. Jesus, F. Zaera, Surf. Sci. 430 (1999) 99.

[61] S. Sambasivan, D. Fischer, B. DeKoven, A. Kuperman, Adv. Mater. 12 (2000) 1890.

[62] P.L. Houston, Chemical Kinetics and Reaction Dynamics, McGraw-Hill, Dubuque, 2001, p. 125.

[63] M. Krivanek, P. Jiru, J. Catal. 27 (1972) 461.

[64] G.S. Wong, J.M. Vohs, Surf. Sci. 498 (2002) 266.

[65] V.V. Pushkarev, V.I. Kovalchuk, J.L. D'Itri, J. Phys. Chem. B 108 (2004) 5341.

[66] T. Ono, K.W. Hillig II, R.L. Kuczkowski, J. Catal. 123 (1990) 236.

[67] M. Imachi, R.L. Kuczkowski, J.T. Grovesand, N.W. Cant, J. Catal. 82 (1983) 335.

[68] T.C. Watling, G. Deo, K. Seshan, I.E. Wachs, J.A. Lercher, Catal. Today 28 (1996) 139.

[69] C. Zhao, I.E. Wachs, Abstracts of Papers, 228th ACS National Meeting, Philadelphia, PA, United States, August 22–26, 2004.

[70] J. Datka, A. Turek, J. Jehng, I.E. Wachs, J. Catal. 135 (1992) 186.

[71] A.J. Turek, I.E. Wachs, E. DeCanio, J. Phys. Chem. 96 (1992) 5000.

[72] M.V. Martinez-Huerta, X. Gao, H. Tian, I.E. Wachs, J.L.G. Fierro, M.A. Banares, The 5G5 Meeting, Catal. Today (special issue), submitted for publication.